Journal of Oceanology and Limnology
Vol. 44, No. 2, pp. 616-633, 2026
https://doi.org/10.1007/s00343-025-5092-2

Research Paper

Decadal trends in particulate organic carbon in the Arabian Sea: biogeochemical drivers across coastal and offshore waters*

Muhsan Ali KALHORO[1, 2, #], Veeranjaneyulu CHINTA[3, #], Muhammad TAHIR[4], Chunli LIU[1], Tony SONG[3], Zhiyuan HE[1], Lixin ZHU[1], Zhenlin LIANG[1, **], Jun SONG[5, 6, 7, 8, **]

[1] *Marine College, Shandong University, Weihai 264209, China*
[2] *Faculty of Marine Sciences, Lasbela University of Agriculture, Water and Marine Sciences, Uthal 90150, Pakistan*
[3] *Ningbo Institute of Digital Twin, Eastern Institute of Technology, Ningbo 315201, China*
[4] *School of Space Science and Technology, Shandong University, Weihai 264209, China*
[5] *Operational Oceanography Institution (OOI), Dalian Ocean University, Dalian 116023, China*
[6] *Dalian Xinghaiwan Laboratory, Dalian 116023, China*
[7] *Liaoning Key Laboratory of Marine Real-Time Forecast and Risk Warning, Dalian 116023, China*
[8] *Dalian Technology Innovation Center for Operational Oceanography, Dalian 116023, China*

Received Mar. 26, 2025; accepted in principle Apr. 24, 2025; accepted for publication Jun. 16, 2025

© Chinese Society for Oceanology and Limnology, Science Press and Springer-Verlag GmbH Germany, part of Springer Nature 2026

Abstract Particulate organic carbon (POC) is a key component of marine carbon cycling. However, its spatiotemporal dynamics in the Arabian Sea remain poorly understood. We investigated the distribution, seasonal variability, and environmental drivers of POC using moderate resolution Imaging Spectroradiometer Aqua (MODIS-Aqua) satellite data (2001–2021) and vertical profiles from the Pelagic Interactions Scheme for Carbon and Ecosystem Studies (PISCES) biogeochemical reanalysis model (Copernicus Marine Services). Surface POC concentrations exhibited profound seasonal variability. Values peaked at 500 mg/m^3 in coastal zones during winter (January–March) and monsoon (July–August). The highest monthly averages were recorded in February (254.8±45.5 mg/m^3), January (208.36±50.2 mg/m^3), and March (196.45±75.3 mg/m^3). Regional analysis revealed distinct patterns: Region A (Pakistan/Iran coast) had winter maxima (504.2 mg/m^3 in January); Region B (Oman) peaked during the monsoon upwelling (835.4 mg/m^3 in July); Region C (India) showed moderate values (327.9 mg/m^3), while Region D (open sea) exhibited stable concentrations (~114 mg/m^3). All regions showed declining POC trends, with the most profound decrease in Region A (-0.28 mg/m^3). Surface POC was strongly correlated with chlorophyll *a* (Chl *a*), at 0.64 in coastal and 0.69 in offshore waters. Vertical profiles revealed strong correlations (>0.8) between POC, Chl *a*, and sea surface temperature (SST). Weaker associations were found with nutrients (NO_3, PO_4), salinity, pH, and oxygen. Seasonal SST maxima (29.1±0.7 °C in May) and deep mixed layers (54.3±5.1 m in January) influenced vertical carbon fluxes. Silicate and oxygen showed depth-dependent patterns. Surface waters were depleted (<2 mmol/m^3), while mesopelagic layers were enriched (20–45 mmol/m^3). This study provided the first integrated satellite-model analysis of POC dynamics in the Arabian Sea. It fills a critical knowledge gap in regional carbon cycling. The findings improved the ability to predict biogeochemical responses to monsoon variability and climate-driven oceanographic shifts, and they also have important implications for global carbon budget estimates.

Keyword: particulate organic carbon (POC); biogeochemical processes; chlorophyll *a*; climate change; Arabian Sea

---

* Supported by the Shandong University, Marine College, Weihai (No. 202367800206), the Science and Technology Plan of Liaoning Province (No. 2024JH2/102400061), the Dalian Science and Technology Innovation Fund (No. 2024JJ11PT007), the Dalian Science and Technology Program for Innovation Talents of Dalian (No. 2022RJ06), the Liaoning Province Education Department Scientific Research Platform Construction Project (No. LJ232410158056), and the Basic Scientific Research Funds of Dalian Ocean University (No. 2024JBPTZ001)

** Corresponding authors: liangzhenlin@sdu.edu.cn; songjun2017@dlou.edu.cn
# Muhsan Ali KALHORO and Veeranjaneyulu CHINTA contributed equally to this work and should be regarded as co-first authors.

1 INTRODUCTION

The carbon cycle in aquatic systems plays a critical role in regulating processes that influence global climate change. In marine environments, organic carbon exists primarily in two forms: dissolved organic carbon (DOC) and particulate organic carbon (POC), which account for approximately 90% and 10% of total organic carbon, respectively (Jahnke, 1996; Loisel et al., 2002). Although POC represents a smaller fraction, it plays a vital role in the "biological pump", a process that transfers carbon from surface waters to the deep ocean, thus supporting the global carbon cycle within marine ecosystems (Ducklow et al., 2001; Honjo et al., 2014; Thomsen et al., 2017). Despite its smaller proportion, POC significantly contributes to carbon export to the deep ocean and serves as a crucial food source within marine food webs (Evers-King et al., 2017). Formed primarily through photosynthesis and solar radiation attenuation, POC plays a key role in the cycling of both DOC and dissolved inorganic carbon (DIC) through the microbial loop (Stramska and Stramski, 2005). It includes both living components, such as phyto-zoo, and bacteria, as well as non-living detritus. POC is widely used as an indicator of biological productivity within the euphotic zone (Fingas, 2019). Understanding the dynamics of POC is essential, as it sustains marine productivity and food webs. POC concentrations are influenced by a range of environmental factors, including phytoplankton biomass, light availability, nutrient levels, salinity, temperature, and chlorophyll-*a* (Chl-*a*) concentrations (Fernandes et al., 2009; Stramska, 2014). Other contributing factors include river discharge (Wang et al., 2012), sediment resuspension (Xu and Milliman, 2009), ocean currents (Fan et al., 2018), and climate variability. Wind speed and tidal forces also play a role in driving water circulation and sediment resuspension, thereby affecting POC levels (Le et al., 2017; Liu et al., 2019). In open oceans, sea surface temperature (SST) can influence POC dynamics by reducing vertical mixing, limiting nutrient availability, and inhibiting phytoplankton growth (Yu et al., 2019). Notably, Chl *a*, a primary source of POC, exhibits a strong positive correlation with POC concentrations (Fernandes et al., 2009).

Remote sensing technology has become important tool for measuring POC concentrations in marine environments. Satellite-based Ocean color sensors, particularly Moderate resolution Imaging Spectroradiometer Aqua (MODIS-Aqua) has been increasingly utilized (Gardner et al., 2006; Son et al., 2009). These sensors estimate POC based on the optical properties of water, relying on the relationship between POC concentrations and the inherent optical properties of the water body. The approach offers key advantages, including large spatial coverage and high temporal resolution, which are difficult to achieve through in-situ methods alone. Although in-situ measurements are generally more accurate, they are costly and offer limited spatial coverage, making them less practical for large-scale or long-term studies (Wei et al., 2019). Satellite measurements, however, can face limitations in optically complex coastal waters, where the presence of both particulate and dissolved substances interfere with the accuracy of retrieval algorithms (Wei et al., 2019; Shaju et al., 2022). To improve the accuracy of satellite-derived POC estimates, especially in under-studied regions like the Indian Ocean, it is essential to integrate satellite data with vertical profile observations. Sources, such as the PISCES biogeochemical model from Copernicus marine services are particularly valuable for this purpose (Świrgoń and Stramska, 2015; Wang et al., 2020). While satellite-based methods have significantly enhanced the global understanding of POC distributions, regional validation remains critical for improving their application in specific local marine environments.

Despite extensive studies on POC distributions in the Pacific, Atlantic and Southern Oceans (Zhu et al., 2011; Stramska, 2014; Fan et al. 2018), relatively limited information exists on POC dynamics in the Indian Ocean, particularly in the northern Arabian Sea (Świrgoń and Stramska, 2015; Shaju et al., 2022). The Arabian Sea is characterized by significant seasonal variability in POC concentrations, which are influenced by atmospheric forcing, oceanic circulation, and biogeochemical processes (Gardner et al., 2006). The Arabian Sea exhibits diverse bathymetric and geological features due to its location at the junction of the Indian, Arabian, and Eurasian plates (Khan and Liu, 2019). The continental shelf is broad off the Indus Delta (up to 130 km) and narrows near the Makran coast (about 20 km) (Mahar, 2010). Features like the Makran Subduction Zone and Murray Ridge, along with freshwater inflow and monsoonal dynamics, significantly influence regional productivity and coastal morphology (Mahar et al., 2019). Freshwater inflow from rivers in both Pakistan and India enhances coastal productivity through enrichment. On the western side, Oman coast benefits from strong monsoon-driven upwelling, supporting high biological productivity (Chinta et al., 2024). This region displays notable seasonal and interannual variability in its physical, biogeochemical properties and Chl-*a* variability (Valsala and Murtugudde, 2015; Kalhoro et al., 2025a). Its marine ecosystem is highly sensitive to global climate change and limited ecological resilience (Johns et al., 2003; Parvaresh et al., 2005). The regions surface dynamics driven by monsoon-related air-sea interactions and heat fluxes. Ekman transport influences open ocean currents, while surface temperatures shaped by local heat exchange (Shetye et al., 1994). Circulation is complex, with frequent eddies (Böhm et al., 1999). The southwest monsoon intensifies boundary currents and induces mixing and Somali upwelling, affected ocean circulations, thermodynamics and decadal climatology (Lee et al., 2000; Chinta et al., 2024). Tropical cyclones also impact this region, altering oceanic conditions such as dissolved inorganic carbon (Kalhoro et al., 2024; Chinta et al., 2025). However, logistical constraints have hindered regular monitoring, resulting in knowledge gaps regarding POC variability and its environmental drivers. The Arabian Sea features unique regional characteristics, including coastal upwelling systems, monsoon-driven seasonal variations, and complex bathymetry. Understanding POC dynamics in this context require integrating various variables, including SST, Chl *a*, sea surface salinity (SSS), and mixed layer depth (MLD), wind, and photosynthetically available radiation (PAR), validating satellite-derived POC data using vertical profile observations from the PISCES biogeochemical model from Copernicus marine services.

To address these knowledge gaps, this study analyzed POC variability in the Arabian Sea using a 20-year dataset (2001–2021). The primary objectives are to assess the spatial seasonal variations of POC and its relationships with key oceanographic variables, such as SST, Chl *a*, SSS, MLD, wind, and PAR. Additionally, the study examines vertical profiles of POC and their controlling factors, including Chl *a*, SST, SSS, nitrate (NO_3), phosphate (PO_4), pH, dissolved oxygen (O_2), and silicate (Si). The Arabian Sea can be divided into four subregions: Region A (Pakistan and Iranian coast), Region B (Oman coast), Region C (Indian coast), and Region D (open waters) to capture the regional variations in POC dynamics. The innovation of this study lies in its integrated approach, combining satellite remote sensing with model-based in-situ measurements of to provide a more comprehensive understanding of POC variability in the Arabian Sea. By analyzing relationships between POC and environmental drivers, the study offers valuable insights into the biogeochemical processes and carbon cycling in this region, thereby contributing to a broader understanding of carbon fluxes in marginal seas and their potential impact on global climate systems.

2 MATERIAL AND METHOD

Twenty years (2001–2021) satellite observation data of standard product for monthly MODIS-Aqua POC and PAR with 4-km resolution was obtained from NASA Ocean Color web platform L3 (https://oceancolor.gsfc.nasa.gov/l3/order/). Chl-*a* data were downloaded from the Copernicus Marine and Environment Monitoring Service (CMEMS) at 4-km×4-km resolution (https://data.marine.copernicus.eu/product/MULTIOBS_GLO_BIO_BGC_3D_REP_015_010/download?dataset=cmems_obs_glo_bgc3d_rep_weekly_202112). Sea surface temperature (SST) data with resolution of 0.05°×0.05° was obtained from CMEMS datasets at https://data.marine.copernicus.eu/product/SST_GLO_SST_L4_REP_OBSERVATIONS_010_011/download?dataset=METOFFICE-GLO-SST-L9994-REP-OBS-SST_202003, sea surface salinity (SSS) datasets at resolution of 0.125°×0.125° was derived from https://data.marine.copernicus.eu/product/MULTIOBS_GLO_PHY_S_SURFACE_MYNRT_015_013/download?dataset=cmems_obs-mob_glo_phy-sss_my_multi_P1M_202311, mixed layer depth (MLD) at resolution of 0.25°×0.25° was also obtained from CMEMS at https://data.marine.copernicus.eu/product/GLOBAL_MULTIYEAR_PHY_ENS_001_031/download?dataset=cmems_mod_glo_phy-all_my_0.25deg_P1M-m_202311. Wind speed (WS) from European Center for Medium-Range Weather Forecasts (ECMWF) database at 0.25°×0.25° resolution (https://cds.climate.copernicus.eu/datasets/reanalysis-era5-single-levels?tab=overview).

The POC was derived using the Blue-Green Band Ratio method (BG Algorithm), a standard empirical algorithm based on NASA Oceancolor protocols. It utilizes the ratio of blue-green spectral reflectance, following the formulation by Stramski et al. (2008) (Eq.1):

$$POC=a\times[(R_{rs(443)}/R_{rs(555)})^{b}]+c, \quad (1)$$

where R is the log-transformed ratio of the reflectance, and a, b, c are the empirical coefficients to be determined.

Chl-*a* concentration was estimated using the Ocean Color sensors (OCx; OC4, OC5 & OC6). algorithm, specifically the equations proposed by O'Reilly and Werdell (2019) (Eqs.2 & 3):

$$\text{Chl } a=10(a+bR+cR^2+dR^3+eR^4), \quad (2)$$

$$R=\log_{10\max}[(R_{rs(443)}/R_{rs(547)}), (R_{rs(488)}/R_{rs(547)})], \quad (3)$$

where a=0.242 4, b=-2.712 3, c=1.801 7, d=-0.001 5, and e=1.228 are the empirically derived coefficients

Vertical profile data for key oceanic parameters were obtained from the Arabian Sea and categorized into four distinct regions: Pakistan and Iranian coast (Region A), Oman coast (Region B), Indian coast (Region C), and Arabian Sea open waters (Region D). These regions were based on different oceanographic processes, coastal activities, river runoff, and bathymetry features (Fig.1). The vertical profiles of including POC, Chl *a*, SST, SSS, pH, NO_3, PO_4, oxygen (O_2), and Si, were derived from the PISCES biogeochemical model, which used the latest version of the Nucleus for European Modelling of the Ocean (NEMO v3.6) simulations. These datasets were retrieved from Copernicus Marine and Environment Monitoring Service (CMEMS). Global ocean biogeochemical hindcasts were produced by Mercator-Ocean, while the nutrient data was compiled from the World Ocean Altas by CMEMS. Heatmaps were generated to investigate the correlations between surface and vertical POC profiles and the associated oceanic parameters across the Arabian Sea and its subregions (https://data.marine.copernicus.eu/product/GLOBAL_MULTIYEAR_BGC_001_029/download?dataset=cmems_mod_glo_bgc_my_0.25deg_P1M-m_202406) (Fig.1).

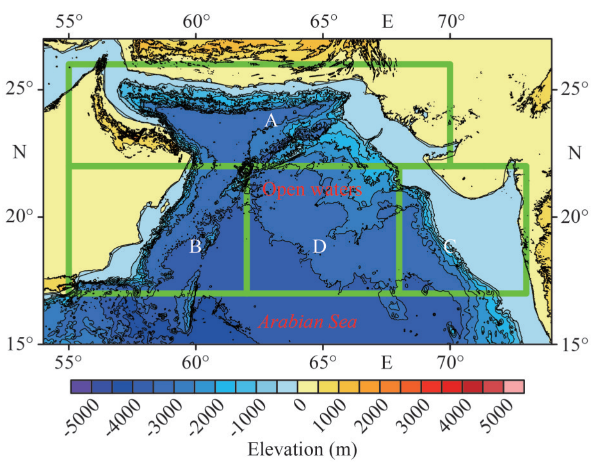

Fig.1 Study area was divided into four regions based on different oceanic and bathymetry conditions of the Arabian Sea

Region A: Pakistan and Iran; Region B: Oman; Region C: India and Pakistan; Region D: Arabian Sea open waters.

Figure 2 illustrates the systematic framework for investigating the dynamics of POC in the Arabian Sea, covering data acquisition, processing, analysis, and interpretation. The study integrated satellite remote sensing data (MODIS-Aqua: POC and PAR; CMEMS: Chl *a*, SST, SSS, MLD, and WS) and

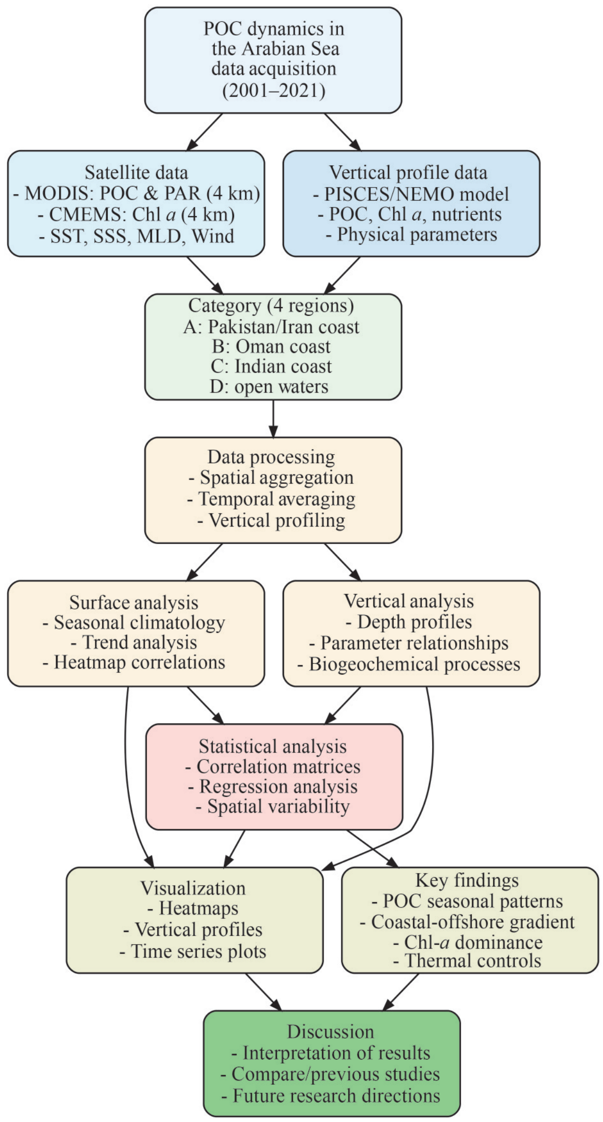

Fig.2 Flowchart outlining the methodology for applying POC dynamics in the Arabian Sea, from data acquisition to discussion and future research directions

vertical profile data from the PISCES/NEMO model reanalysis data from 2001 to 2021. These datasets categorized into four distinct regions, the Pakistan/Iran coast, Oman coast, Indian coast, and open waters, allowing for a comprehensive regional analysis. The data underwent multiple processing steps, including spatial aggregation, temporal averaging, and vertical profiling. Analytical procedures focused on both surface and subsurface patterns through seasonal climatologies, trend analysis, heatmap-based correlations, depth profile assessments, parameter relationships, and biogeochemical processes. Key findings, such as thermal regulation of POC dynamics, were identified. The results were effectively visualized using spatial maps, heatmaps, and vertical cross-sections. The flowchart represents a structured, coherent, and comprehensive methodological approach to understanding the variability and controlling factors of POC in the Arabian Sea.

3 RESULT

3.1 Spatial distribution of POC

The monthly average climatology of surface POC concentrations in the Arabian Sea from 2001 to 2021 reveals a dynamic seasonal cycle. POC concentrations ranged from 10 to 500 mg/m^3, with distinct seasonal peaks and troughs observed in both coastal and offshore regions (Fig.3). The highest POC concentrations were occurred in February, January, and March, with averages of 254.80±45.5, 208.36±50.2, and 196.45±75.3 mg/m^3, respectively. The maximum POC values reached 332.68 in February and 339.85 mg/m^3 in March, while minimum values were relatively high, ranging from 179.72 in February to 143.19 mg/m^3 in January. The highest concentrations were observed along the coast, while offshore regions exhibited moderate levels. Notably, March (±75.3 mg/m^3) and August (±65.2 mg/m^3) showed the highest variability in POC concentration, whereas the most stable conditions were observed in October (±30.9 mg/m^3) and November (±25.7 mg/m^3). In contrast, the lowest POC levels were observed in April, May, and June, with average concentrations of 123.89±35.7, 118.52±40.1, and 125.64±45.9 mg/m^3, respectively. During these months, the minimum values ranged between 181.54 in April and 263.7 mg/m^3 in May. These climatological variations highlight significant oceanographic and biogeochemical influences on POC distribution (Fig.3).

3.2 Spatial distribution of Chl *a*

The monthly climatology of surface Chl-*a* concentration in the Arabian Sea from 2001 to 2021 reveals a distinct seasonal cycle (Fig.4). The lowest average Chl-*a* concentrations were recorded in April

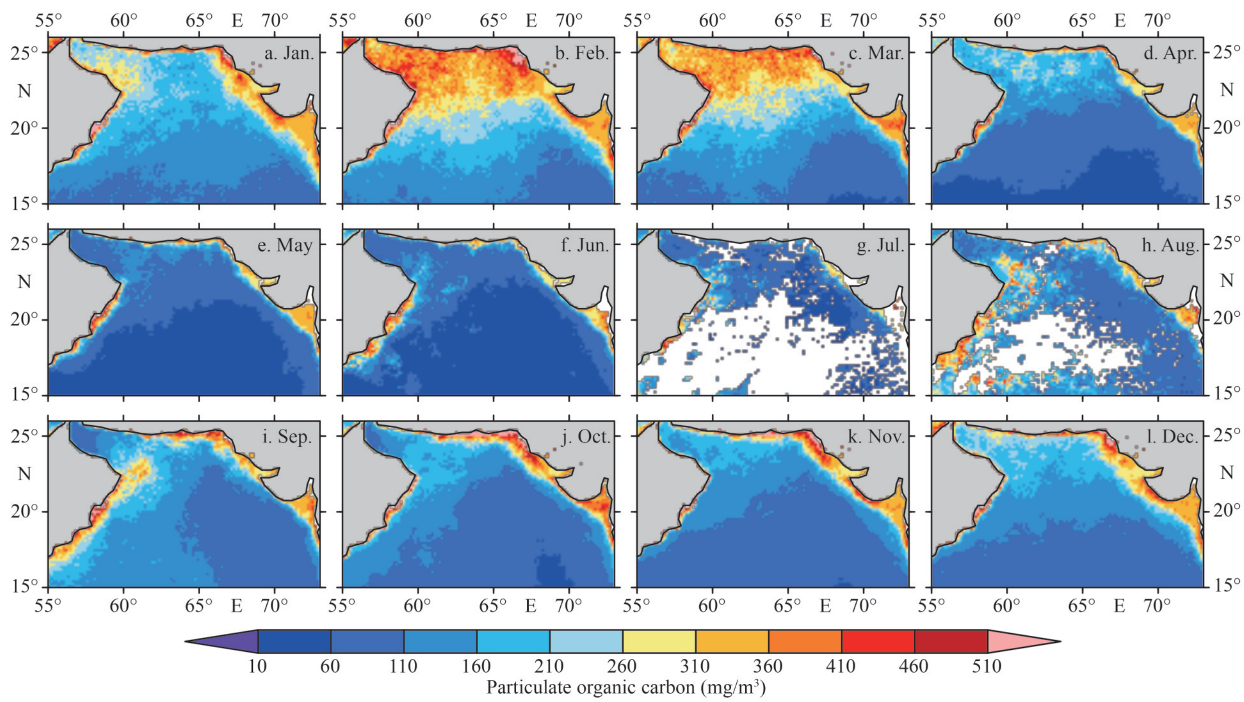

Fig.3 Surface mean climatology of POC (mg/m^3) variability in the Arabian Sea during 2001–2021

(0.67±0.15 mg/m^3) and May (0.64±0.12 mg/m^3), with minimum values reaching 0.42 mg/m^3 in both months, and maximum values remaining below 1 mg/m^3. Similarly, November (0.93±0.18 mg/m^3) also showed relatively low Chl-*a* levels, indicating minimal phytoplankton productivity during these periods. In contrast, the highest average Chl-*a* concentrations were observed in August (1.89± 0.61 mg/m^3) and February (1.82±0.45 mg/m^3), with maximum values reaching 2.57 and 2.92 mg/m^3, respectively. These peaks suggest enhanced biological activity, possibly influenced by monsoonal dynamics and nutrient availability (Fig.4). The variability in Chl *a* was most pronounced in July (±0.72 mg/m^3) and August (±0.61 mg/m^3), indicating substantial fluctuations in phytoplankton biomass during these months. In contrast, May (±0.12 mg/m^3) and April (±0.15 mg/m^3) exhibited the most stable conditions, with minimal deviations from the average. The highest levels were observed along the coasts of Pakistan, India, and Oman, attributed to nutrient-rich waters and upwelling zones. These seasonal trends highlight the influence of oceanographic and climate factors on Chl-*a* distribution, reflecting the productivity dynamics within the Arabian Sea (Fig.4).

3.3 Sea surface temperature (SST) climatology

The monthly average climatology of SST in the Arabian Sea reveals distinct seasonal pattern, influenced by combination of oceanographic and climate factors (Fig.5). The highest average SST was recorded in May (29.12±0.73 °C) and June (28.97±0.81 °C). During these months, SST ranged between 28.05 °C and 30.48 °C, reflecting peak warming conditions. Similarly, October (28.67± 0.42 °C) and April (27.89±0.59 °C) also showed relatively high SST values, indicating the transition to warmer conditions. In contrast, the lowest average SST were observed in February (24.82± 0.52 °C) and January (24.98±0.45 °C), with minimum temperatures reaching 23.97 °C and 24.24, respectively. December (26.23±0.33 °C) also marked cooler period, maintaining relatively lower temperatures compared to mid-year months. The greatest SST variability, indicated by standard deviation, was recorded in June (±0.81 °C) and May (±0.73 °C), suggesting dynamic oceanographic conditions during the early summer months. Conversely, December (±0.33 °C) and November (±0.38 °C) exhibited the least variation, indicating more stable temperature patterns (Fig.5). Upwelling slightly reduces SSTs near the coast, despite the overall high temperatures in the region. These fluctuations in SST reflect seasonal climate influences, including monsoonal variations, solar radiation intensity, and oceanic circulation patterns, shaping the thermal structure of the Arabian Sea.

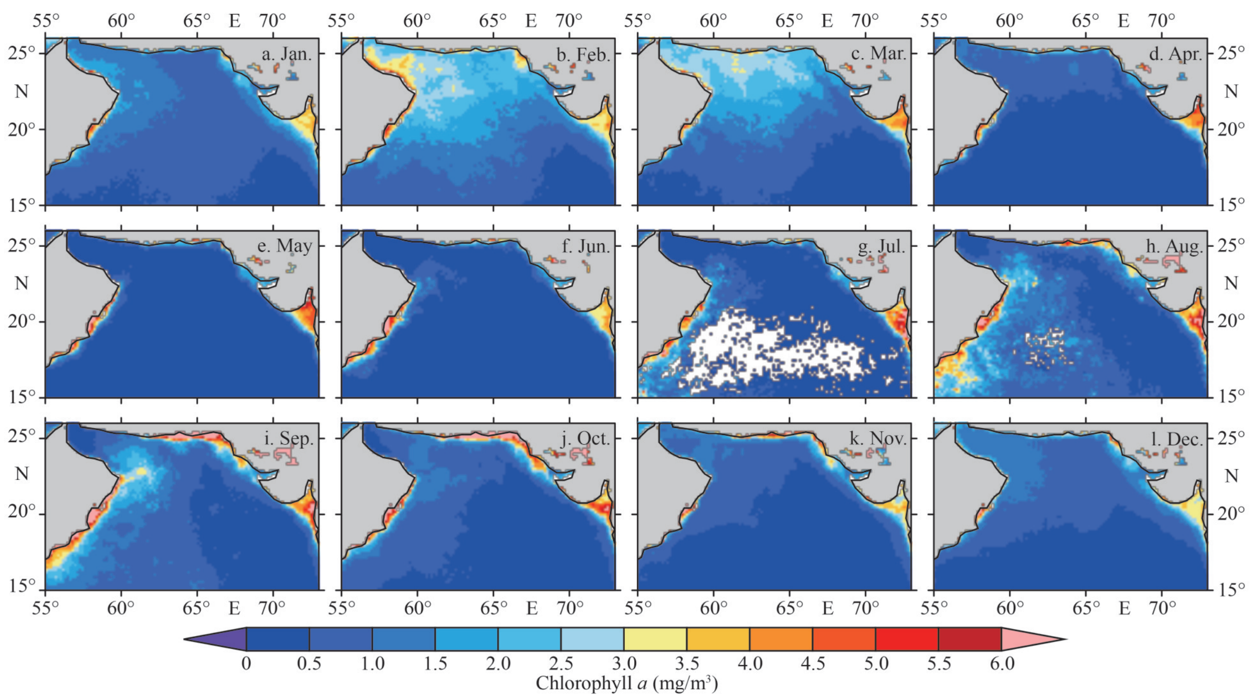

Fig.4 Monthly average climatology of Chl-*a* concentration (mg/m^3) during 2001–2021 in the Arabian Sea

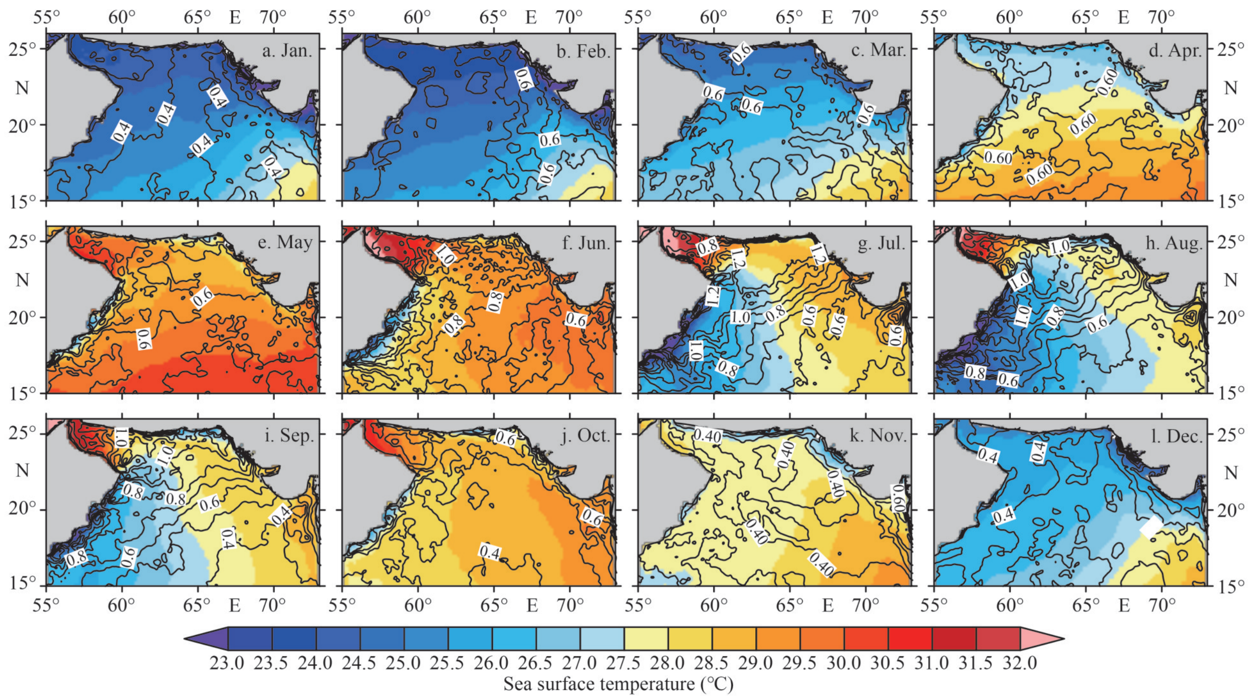

Fig.5 Spatial distribution of monthly mean SST (°C) climatology during 2001–2021 in the Arabian Sea

3.4 Sea surface salinity (SSS) pattern

SSS is a key parameter for understanding the hydrological cycle, ocean circulation, and the influence of freshwater inputs from precipitation and river discharge. The seasonal and monsoonal variations in SSS are shown in Fig.6. The highest average salinity levels were observed in May (36.47±0.09) and June (36.44±0.13), with values ranging between 36.16 and 36.61, indicating peak salinity during the pre-monsoon period. Similarly, April (36.39±0.14) and August (36.42±0.09) also exhibited elevated salinity levels. The lowest values were recorded in December (36.30±0.09), February (36.32±0.06), and November (36.32±0.08), with minimum values dropping to 36.14 in December and 36.17 in November. March (36.33±0.12) and January (36.33±0.08) showed similar salinity conditions, reflecting the stable influence of oceanographic processes. The highest variability in salinity, as indicated by the standard deviation, was noted in April (±0.14) and June (±0.13), suggesting dynamic oceanographic influences during the transitional months. In contrast, February and October (±0.06) exhibited the least variation, indicating more stable conditions. Higher SSS values were observed moving from Iranian waters to the offshore regions, with the highest values occurring during the summer months and gradually decreasing during the winter months (Fig.6). Overall, these salinity fluctuations are influenced by seasonal factors such as monsoon-driven precipitation, riverine freshwater input, and evaporation rate, shaping the SSS structure in the Arabian Sea.

3.5 MLD climatology

The average monthly climatology of the MLD in the Arabian Sea exhibits distinct seasonal variability, influenced by oceanic stratification and monsoon-driven process (Fig.7). The deepest mixed layers were recorded in January (54.32±5.12 m) and December (43.25±4.56 m), with maximum values reaching 63.95 and 53.16 m, respectively. Indicating stronger convective mixing during winter (Fig.7). During the summer monsoon (June–August), the MLD varied, with June (21.34±2.78 m), July (27.45±3.45 m), and August (25.98±2.89 m) showing moderate depths, reflecting increased wind-driven mixing. The shallowest mixed layers were observed in April (15.12±1.89 m) and May (17.89±1.95 m), coinciding with the pre-monsoon stratification, when the MLD was at its lowest due to higher surface heating and reduced turbulence. The post-monsoon period (September–November) exhibited increasing MLD values, with November (28.45±3.12 m) showing significant deepening. The highest variability in MLD was observed in

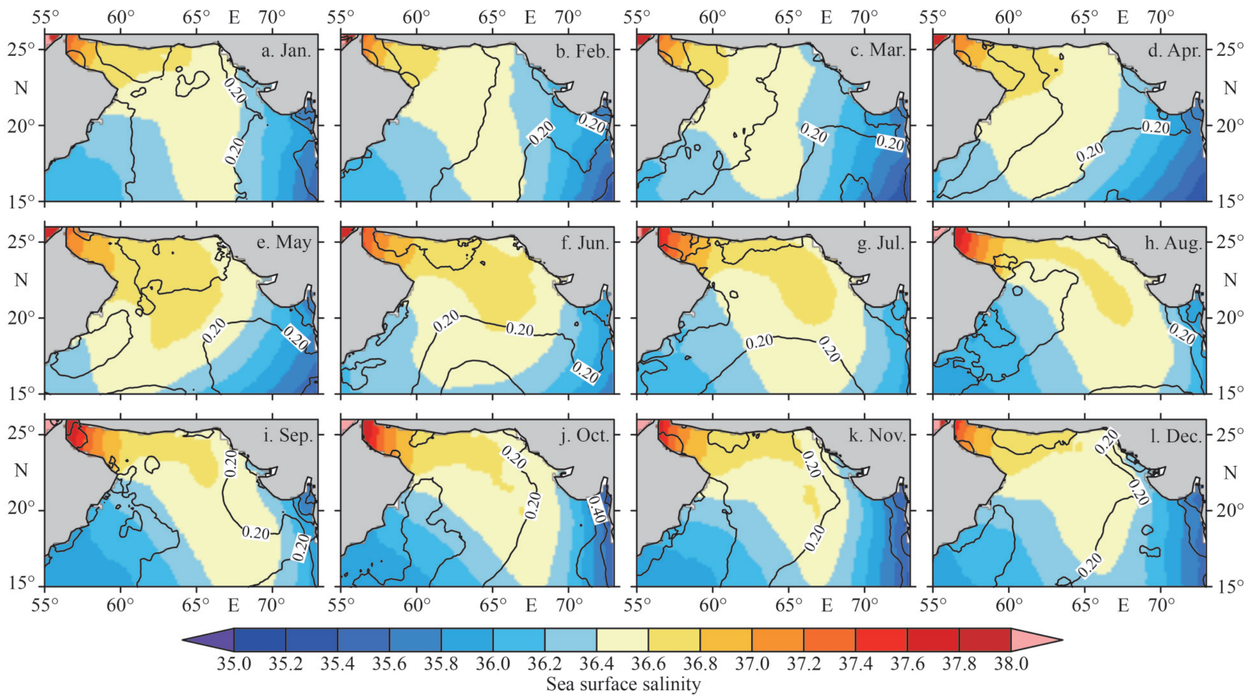

Fig.6 Spatial distribution of monthly mean climatology of SSS masses during 2001–2021 from the Arabian Sea

February (40.87±9.45 m), likely due to transitional oceanographic conditions (Fig.7). Overall, the seasonal MLD changes are driven by monsoon dynamics, heat flux variations, and wind-induced mixing, shaping the vertical structure of the upper ocean in the Arabian Sea.

3.6 Variable climatological relationship

Seasonal variations in POC, Chl *a*, SST, SSS, and MLD in the Arabian Sea are strongly influenced by monsoonal dynamics. A positive correlation between POC and Chl *a* is observed, particularly during the summer monsoon (June–August) and

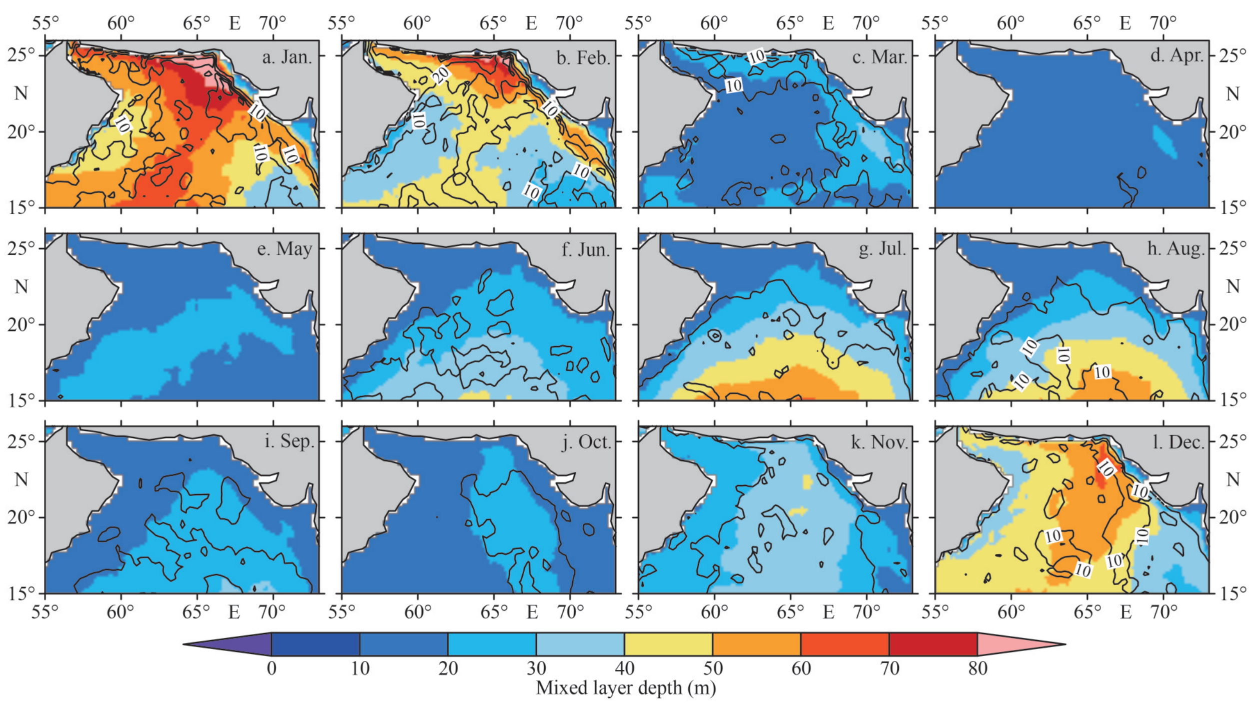

Fig.7 MLD (m) monthly mean climatology variations in the Arabian Sea in the last two decades

post-monsoon (September–November) periods. Peak Chl-*a* concentrations of 1.89±0.61 in August and 1.65±0.72 mg/m^3 in July align with increase POC levels. SST affects productivity, with cooler temperature during the monsoon (~26–27 °C) correspond with higher Chl *a* due to nutrient enrichment, while higher SST (~29–30 °C) during pre-monsoon limits productivity. MLD variations also play a key role deeper MLDs in January (54.32± 5.12 m) and December (43.25±4.56 m) enhance nutrient supply, supporting moderate Chl-*a* concentrations, while shallower MLDs in April (~15.12 m) coincide with lower Chl-*a* levels. SSS remain relatively stable (~36.3–36.5) but shows a minor seasonal variation. Higher salinity in May–June (~36.47) contributes to surface layer stability, while lower SSS during the monsoon (~36.32 in November) facilitates nutrient mixing. The high WS were observed during the summer months starts from May to September, lower in winter months from the study area (Supplementary Fig.S1), while the highest PAR starts during March–July and become low started from August to onward months (Supplementary Fig.S2). These relationships emphasize the critical role of monsoonal forcing, with stronger mixing and cooler SSTs during the monsoon supporting higher productivity and nutrient availability, while warmer SSTs and shallow MLDs during the pre-monsoon reduce productivity. Monthly surface time series of key oceanic parameters reveal overall variability across the Arabian Sea. Understanding these dynamics is essential for assessing ecosystem responses to climate variability (Supplementary Fig.S3).

3.7 Correlation between POC and key oceanic variable

The correlation matrix revealed significant relationships between POC and key oceanic variables, highlighting complex biogeochemical and physical interactions in the marine environment (Table 1). POC exhibited a strong positive correlation with Chl *a* (0.64, $P<0.05$), indicating a strong coupling between phytoplankton biomass and organic carbon production. Conversely, POC showed a robust negative correlation with SST (-0.72, $P<0.05$), suggesting that warmer waters suppress POC accumulation, possibly due to enhanced stratification. POC also displayed moderate negative correlations with SSS (-0.35), PAR (-0.36), and WS (-0.33), implying that fresher, calmer, and lower-light conditions favored POC retention (Table 1). Conversely, POC was positively correlated with MLD (0.43), highlighting the role of deeper mixing in redistributing organic carbon from subsurface layers. Notably, SST showed a strong negative correlation with MLD (-0.72), consistent with thermal stratification that inhibited vertical mixing. This stratification likely reduced nutrient availability, as reflected in SST inverse relationship with Chl *a* (-0.50), suggesting that elevated temperatures suppressed phytoplankton productivity. PAR exhibited a pronounced inverse correlation with MLD (-0.73), suggesting that deeper mixed layers reduced light penetration and potentially limited photochemical processes. The positive correlation between SST and PAR (0.50) further supported the interplay between surface warming, stratification, and light attenuation. SSS was positively correlated with both SST (0.32) and WS (0.48), indicating that wind-driven mixing and evaporation in warmer regions enhanced surface salinity (Table 1). The weak but noticeable relationship between WS and Chl *a* (0.13) suggested limited wind-driven nutrient entertainment in the system. Collectively, these correlations emphasized the dominance of thermal stratification (SST-MLD dynamics) and biological productivity (Chl *a*-POC linkage) in regulating POC distribution, with secondary influences from salinity gradients, light availability, and wind-driven physical processes.

3.8 Regional monthly POC time series variability

Analysis of monthly mean POC climatology across four regions of the Arabian Sea reveals distinct seasonal cycles, characterized by winter maxima driven by convective mixing and summer minima associated with stratified, oligotrophic conditions. Region A exhibited the highest winter peaks, particularly in February 2003 (504.22 mg/m^3), February 2005 (488.63 mg/m^3), and March 2001

Table 1 Correlations between POC and key oceanic drivers in the Arabian Sea

Variable	POC	Chl *a*	SST	SSS	MLD	PAR	WS
POC	1	0.645	-0.721	-0.349	0.428	-0.365	-0.327
Chl *a*	0.645	1	-0.493	-0.079	0.173	-0.223	0.131
SST	-0.721	-0.493	1	0.363	-0.724	0.497	0.266
SSS	-0.349	-0.079	0.363	1	-0.189	0.305	0.480
MLD	0.428	0.173	-0.724	-0.189	1	-0.728	-0.153
PAR	-0.365	-0.223	0.497	0.305	-0.728	1	0.207
WS	-0.327	0.131	0.266	0.480	-0.153	0.207	1

(499.95 mg/m^3), with concentrations consistently exceeding 400 mg/m^3 during the January–March. Summer minima in this region dropped significantly, ranging 74.86–90.91 mg/m^3 (June–July, 2015–2018), yielding an annual mean of 217.04±93.13 mg/m^3 (Table 2). The decreasing annual trend (-0.28 mg/m^3) was observed in this region. Region B displayed profound interannual variability, with notable peaks in July 2020 (835.43 mg/m^3) and June 2005 (602.85 mg/m^3), alongside winter maxima in January–March 2009 (598.58–707.95 mg/m^3). Conversely, summer-autumn troughs reached as low as 8.20 mg/m^3 (October 2021), reflecting episode nutrient limitation. The regional average (187.07±92.82 mg/m^3) underscores its transitional biogeochemical regime. Region C showed moderate seasonality, with winter-spring maxima (January 2001: 327.87 mg/m^3; May 2012: 301.07 mg/m^3) and summer-autumn minima (March 2016: 53.82 mg/m^3; October 2012: 67.15 mg/m^3) in average of 146.29±52.13 mg/m^3. In contrast, Region D (offshore) exhibited the lowest annual mean (114.17±52.52 mg/m^3), peaking in February 2020 (307.70 mg/m^3) and May 2012 (298.53 mg/m^3) but declining to ≤44.75 mg/m^3 during summer stratification (September 2008–2013). Overall decreasing trend in POC concentration were observed in all regions of Arabian Sea, highest in Region A (Table 2 & Supplementary Fig.S4).

Notably, all regions followed a winter-high, summer-low trend, with coastal zones (Region A) demonstrating the strongest seasonal amplitude. This gradient is attributed to intensified winter mixing and monsoonal nutrient inputs, particularly from the Indus Delta, which elevates coastal productivity. Region B episodic peaks likely reflect dust-driven fertilization from arid regions, while offshore areas remain nutrient-limited outside winter mixing periods. These findings highlight the critical roles of terrestrial inputs, monsoonal hydrodynamics, and regional bathymetry in shaping the carbon dynamics of the Arabian Sea.

3.9 Regional Chl-*a* concentration

Chl-*a* concentration across the Arabian Sea displayed a profound coastal-offshore gradient, with seasonal peaks driven by monsoon-mediated dynamics. Region A showed winter maxima (February 2006: 4.60 mg/m^3), and summer minima (July 2012: 0.29 mg/m^3), resulting annual mean of 1.42±0.78 mg/m^3, indicative of pre-monsoon productivity. Region B exhibited extreme variability, with upwelling-driven peaks in October 2005 (6.59 mg/m^3) and March 2017 (6.37 mg/m^3), contrasting with post-monsoon lows in November 2016 (0.51 mg/m^3), mean of 1.59±1.14 mg/m^3. Region C recorded moderate pre-monsoon maxima (March 2004: 3.01 mg/m^3) and a mean of 1.10± 0.30 mg/m^3. Offshore Region D showed late monsoon peaks (October 2015: 2.94 mg/m^3) but maintained a low annual mean of 0.62±0.47 mg/m^3, with values suppressed to ≤0.08 mg/m^3 during summer stratification (Table 2 & Supplementary Fig.S4). These spatial-temporal patterns underscore the critical role of monsoon-driven nutrient fluxes and coastal upwelling regulating phytoplankton biomass variability

3.10 Regional SST time series

SST across the Arabian Sea regions exhibited marked seasonality, with summer maxima (June–July: 29–31 °C) and winter minima (February: 22.6–22.8 °C). Region A recorded the highest summer peaks (31.3 °C in 2020) and averaged 27.16± 2.11 °C. Region B, the coldest region, showed moderate variability (mean: 26.46±1.55 °C), while Region C (27.96±1.33 °C) and D (27.30±1.46 °C) mirrored seasonal trends. Overall, SST averaged 27.22 °C, underscoring the thermal homogeneity of offshore zones and coastal warming disparities driven by monsoonal mixing and solar forcing (Table 2 & Supplementary Fig.S4).

3.11 Regional SSS time series

The SSS across regions exhibited minor veracity, with coastal-offshore gradients. Region A (mean: 36.68±0.10) peaked at 37.01 (September 2016), while Region C recorded the lowest averaged salinity 35.22 (May 2018) and highest variability (36.11±0.24). Region B (36.29±0.14) and D (36.45± 0.11) showed relative stability, with maxima in summer (36.60–36.79) and minima during monsoon months (35.92–35.99). The patterns reflect monsoonal freshwater influx in coastal zones (A, C) and evaporative dominance in offshore regions (D) (Table 2 & Supplementary Fig.S4).

3.12 Regional MLD time series

The MLD across the Arabian Sea exhibited pronounced seasonal variability, driven by monsoonal winds and stratification cycles. Region A showed the deepest winter MLD (January 2014: 77.3 m) and shallowest summer MLD (April 2020: 11.5 m), averaging 25.86±16.55 m. Region B

Table 2 Descriptive statistics for various environmental variables from different regions of the Arabian Sea

Variable	Statistics	Region			
		A	B	C	D
POC (mg/m^3)	Average	217.04	187.07	146.30	114.17
	SD (±)	93.13	92.82	52.13	52.52
	Min	74.86	8.20	53.82	37.18
	Max	504.21	835.43	327.87	307.70
	Trend	-0.28	-0.19	-0.16	-0.08
Chl *a* (mg/m^3)	Average	1.42	1.54	1.10	0.62
	SD (±)	0.78	1.14	0.30	0.47
	Min	0.294	0.505	0.18	0.08
	Max	4.60	6.59	3.01	2.94
SST (°C)	Average	27.16	26.46	27.96	27.30
	SD (±)	2.11	1.55	1.33	1.46
	Min	22.63	23.4	24.67	24.11
	Max	31.31	29.79	30.56	30.7
SSS	Average	36.68	36.29	36.11	36.45
	SD (±)	0.10	0.13	0.23	0.11
	Min	36.37	35.99	35.22	35.92
	Max	37.01	36.60	36.62	36.79
MLD (m)	Average	25.86	25.65	26.36	31.43
	SD (±)	16.55	11.17	9.57	13.87
	Min	11.49	11.29	12.47	11.99
	Max	77.30	57.84	56.35	72.19

mirrored this trend, with July 2019 peaks (57.8 m) and summer minima (August 2012: 11.3 m; mean 25.65±11.17 m). Region C displayed summer maxima (July 2010: 56.4 m) and winter lows (January 2018: 12.5 m; mean 26.36±9.57 m). Region D recorded the deepest overall MLD (September 2015: 72.2 m) and highest average (31.87±13.87 m), contrasting sharply with March 2011 stratification (12.0 m). Coastal regions showed stronger seasonal MLD fluctuations, while offshore regions reflected prolonged mixing influenced by open-ocean dynamics (Table 2 & Supplementary Fig.4).

3.13 Vertical profile of environmental variable

The vertical profiles reveal pronounced gradients in biogeochemical parameters across the Arabian Sea. Surface mean POC concentrations peaked at >50 mg/m^3 (0–50 m), declining to <21 mg/m^3 at 100 m, with a mid-depth resurgence (150–350 m: > 5 mg/m^3) linked to particle sinking. Regions A and B exhibited the highest integrated POC, while region C showed elevated subsurface values, despite lower surface concentrations (Fig.8). Chl *a* displayed distinct zonation, with maxima (0.2–0.4 mg/m^3) in the euphotic zone (10–60 m), plummeting to <0.07 mg/m^3 below 100 m. Region B dominated surface productivity (Chl *a*>0.4 mg/m^3), contrasting with surface values in region C (<0.2 mg/m^3). Thermal stratification was evident, with surface SST>26 °C (up to 50 m), peaking in region C (27.98 °C). Temperatures declined steeply below 100 m, reaching <14 °C at 450 m. Salinity profiles highlighted coastal-offshore contrasts. Region A (surface: 36.57), exceeded Region C (35.95±0.22), which showed mid-depth enrichment (>36 at 50–300 m) (Fig.8).

Nutrient distribution mirrored classic oligotrophic trends: surface NO_3 and PO_4 were depleted (<1 mmol/m^3) but surged with depth, exceeding 11 (NO_3) and 2.0 mmol/m^3 (PO_4) below 500 m. region C and D had higher deep NO_3, while region B exhibited elevated PO_4. Surface pH (>8.0) declined with depth, reaching <8.0 in mesopelagic layers, with region B exhibiting slightly lower surface pH. Dissolved oxygen maxima (>200 mmol/m^3; 0–50 m) decreased sharply to <2.0 mmol/m^3 at 500 m, with region A retaining higher subsurface oxygen. Si concentrations increased uniformly with depth (2 mmol/m^3 at surface; 20–45 mmol/m^3 at 150–500 m), showing negligible regional variations (Fig.8). These profiles underscore the interplay of physical stratification, coastal inputs, and biological activity in shaping carbon and nutrient cycling, with implications for regional productivity and export fluxes.

3.14 Regional surface POC and its controlling factors

The correlation analysis (Table 3) delineates regional drivers of surface POC variability from 2001 to 2021. In regions A (coastal) and D (offshore), Chl *a* exhibiting the strongest positive corrections (R^2>0.6), underscoring phytoplankton biomass and the dominant carbon source. Moderate SST-POC linkages (R^2>0.5) in Regions A and C highlight the thermal regulation of biological processes, while SSS showed negligible influence (R^2<0.3) across all regions. Notably, Region C uniquely displayed MLD-POC coupling (R^2>0.5), likely driven by wind-driven mixing replenishing surface nutrients

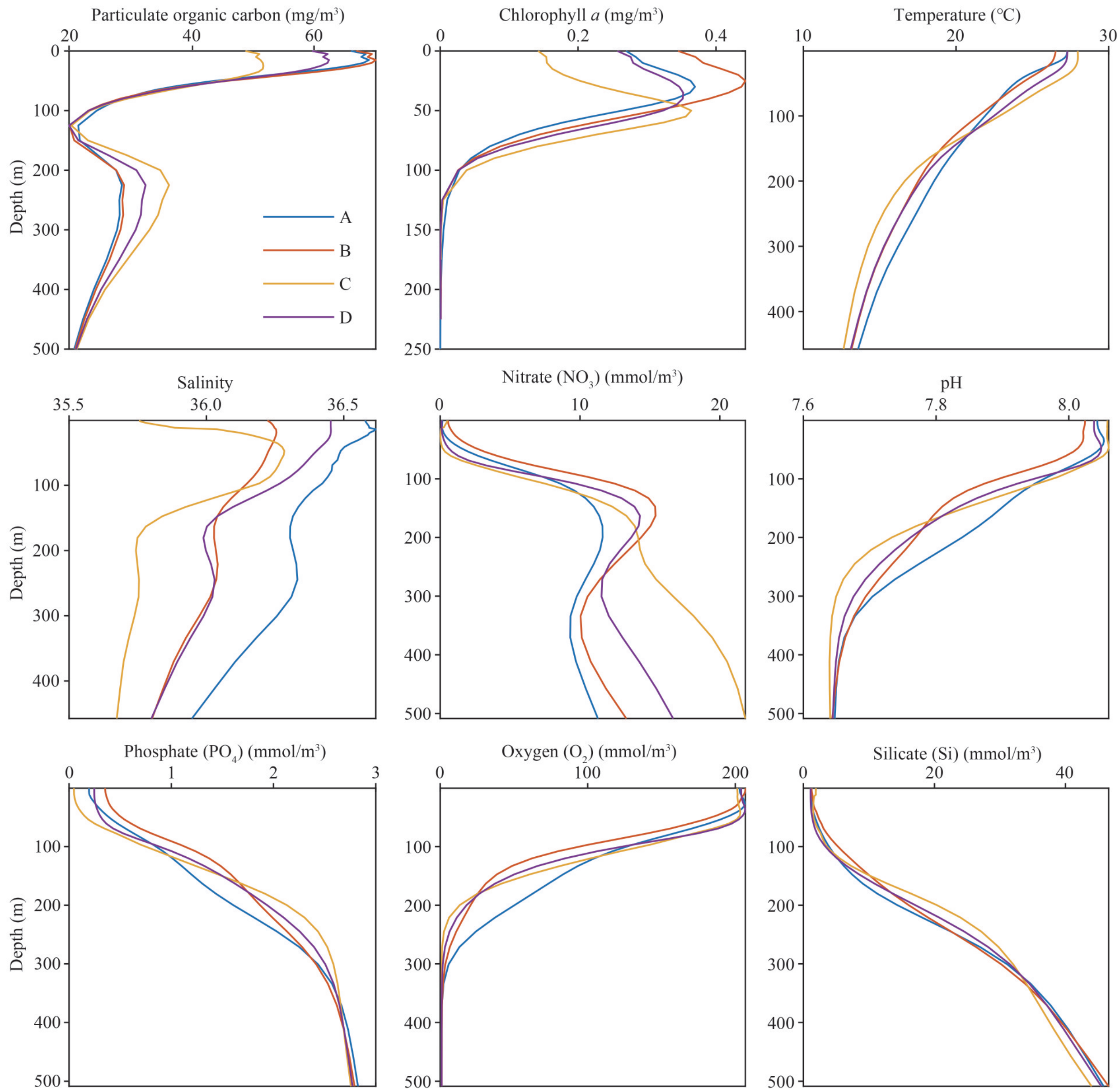

Fig.8 Vertical profile variability of oceanic parameters from different regions of the Arabian Sea during 2001–2021

(Table 3). These contrasts emphasize region-specific drivers: coastal zones (Region A) are governed by productivity and temperature, offshore regions (Region D) by Chl-*a* dynamics, and transitional zones (Region C) by physical mixing. The findings underscore the primary production and hydrographic processes in modulating Arabian Sea carbon fluxes, with implications for refining regional carbon cycling models under climate change scenarios.

3.15 Vertical POC profile and correlation with driving factors

Heatmap analysis of vertical POC concentrations (Fig.9) highlights region-specific drivers of carbon variability. Chl *a* dominates in coastal regions (Region A) (0.845) and B (0.906), affirming phytoplankton biomass as the principal regulator of POC. Offshore Region D similarly exhibited strong Chl *a*-POC coupling (0.765), while in Region C, SST was the primary driver (0.421), suggesting

Table 3 Surface POC correlation (R^2) with key oceanic drivers across different regions

Region	Chl *a*	SST	SSS	MLD
A	0.637	0.54	0.179	0.191
B	0.436	0.258	0.050	0.010
C	0.124	0.525	0.033	0.299
D	0.690	0.497	0.048	0.080

thermal regulation of microbial degradation or particle aggregation processes. SST demonstrates moderate influence in Regions A (0.677) and D (0.469), reflecting temperature-dependent metabolic processes. Nutrients, NO_3, PO_4, pH, O_2, and Si, exhibited negligible correlations (<0.4) across all regions, indicating minimal direct control on vertical POC distribution. Region B weak SSS-POC linkage (0.386) contrasts with coastal Region A (0.520), due likely to terrestrial runoff impacts. The stark regional contrasts coastal zones dominated by productivity drivers and offshore areas influenced by Chl *a*/SST interplay underscore the complexity of depth-dependent carbon flux regulation. These findings emphasize phytoplankton dynamics and thermal stratification as pivotal to vertical POC structuring, offering critical insights for modeling carbon export pathways in heterogeneous marine systems (Fig.9).

4 DISCUSSION

Satellite remote sensing plays a critical role in elucidating marine carbon dynamics across diverse spatiotemporal scales. The Arabian Sea, driven by monsoons, coastal upwelling, and land-derived inputs, offers a dynamic environment for examining POC variability. This study examines the spatial, vertical, and temporal patterns of POC in coastal and offshore regions, offering insights into the interplay of physical and biological drivers influencing carbon fluxes. Coastal regions exhibited elevated POC concentrations (100–500 mg/m^3),

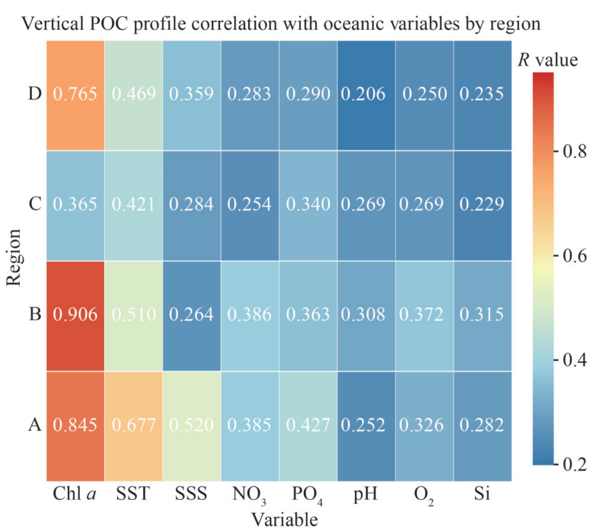

Fig.9 Heatmap of correlation coefficients for vertical POC profiles and key oceanic variables in four different regions of the Arabian Sea

primary driven by terrestrial runoff, riverine discharge (e.g., Indus River), and hydrodynamic processes. This gradient diminished offshore (10–60 mg/m^3), reflecting reduces land-derived nutrient inputs, consistent with global observations in the Bay of Bengal and Yellow Sea (Fan et al., 2018; Kandasamy et al., 2019). The climatology analysis (2001–2021) revealed pronounced seasonality: surface POC peaked during winter (January–March, 196–255 mg/m^3) due to convective mixing, while the southwest monsoon (June–August) enhanced coastal POC (400–500 mg/m^3) via upwelling-induced productivity. Offshore zones, however, experienced suppressed POC during this period, likely due to oligotrophic conditions. These patterns align with monsoon-mediated nutrient cycling in the Bay of Bengal (Dobashi et al., 2022), contrasting with South Pacific trends, where POC levels rise due to increased Chl-*a* levels (Stramska and Cieszyńska, 2015). Regionally, POC concentrations declined from coastal (Region A: 217.05 mg/m^3) to offshore waters (Region D: 114.17 mg/m^3), reflecting similar gradients observed in the north Atlantic and Jiaozhou Bay (Yu et al., 2019; Shen et al., 2020). The presence of sediment and particles at coastal waters also contributes to the variability of POC optical proxies (Karp-Boss et al., 2004; Holser et al., 2011). Notably, Region A exhibited the steepest negative trend (-0.280/a), attributed to anthropogenic stressors and warming-induced declines in productivity (Roxy et al., 2016). Similar declines observed in the Bay of Bengal (-1.12/a) and Atlantic Ocean (-1.08–-0.10/a) underscore global shifts in marine productivity, though regional drivers vary (Stramska, 2014; Rouf et al., 2021).

Vertical POC profiles showed surface maxima (0–50 m) with a secondary peak at 150–350 m, indicative particle aggregation and zooplankton-mediated export (Roman et al., 2000). Subsurface enrichment aligns with prior sediment trap studies in the northern Arabian Sea, where fecal pellet fluxes dominate carbon export (Sarin et al., 1996). Regions A and B exhibited higher subsurface POC, likely due to intense coastal upwelling and microbial remineralization. The rapid decline in Chl *a* below 60 m underscored the decoupling of primary production and carbon export, with smaller phytoplankton dominating post-monsoon periods, reducing particle sinking rates (Bhattathiri et al., 1996; Ramaiah et al., 1996). POC concentration in the ocean exhibit significant spatial, vertical, seasonal, and annual variations (Stramska, 2009, 2014; Fan et al., 2018; Yu et al., 2019).

Chl-*a* concentrations mirrored monsoon-driven productivity, peaking during the southwest monsoon (>5 mg/mg^3) due to nutrient-rich upwelling, while winter mixing sustained moderate levels. Region B recorded the highest Chl *a* (1.59 mg/m^3), reflecting its transitional biogeochemical status between coastal eutrophy and offshore oligotrophy. The coastal regions, serving as transition between nearshore and offshore waters, exhibited distinct biogeochemical processes (Giraud et al., 2008). The declining POC gradient from coastal to offshore regions reflects the diminishing influence of terrestrial and riverine inputs in ocean environments (Gomes et al., 2000; Gopalakrishna et al., 2002; Fernandes et al., 2009). Arabian Sea productivity exceeds that of the Bay of Bengal, owing to dust deposition from arid regions and persistent upwelling (Patra et al., 2007). However, declining Chl-*a* trends reported by Prakash et al. (2012) suggest evolving nutrient limitations under warming scenarios. SST remains a key factor in understanding marine ecosystems, as it influences primary production and overall ocean health including red tides (Chiswell and Sutton, 2020; Liu et al., 2025). SST and MLD exert strong controls on POC dynamics. Winter cooling (23–25 °C) enhanced vertical mixing, enriching surface nutrients, while summer stratification (30–32 °C) limited offshore productivity. SST trends in the Arabian Sea outpace global averages, exacerbating thermal stratification and potentially reducing future carbon export (Fox-Kemper et al., 2021). Salinity remained spatially homogenous (36.11–36.68), reflecting balanced evaporation and advective processes. Similar decreasing SSS trend with depth was observed in prior studies (Kalhoro et al., 2025b). MLD in the Arabian Sea varied seasonally, being deepest in winter (60–80 m) due to convective mixing and shallower in spring and post-monsoon periods (10–30). During the monsoon, MLD ranged from 40 to 60 m, facilitating nutrient upwelling and boosting coastal productivity. The average MLD was 25.86 m in Region A and 31.87 m in Region D, with deeper mixing in the open ocean. These seasonal changes in MLD are crucial for regulating Chl-*a* concentrations, aligning with prior studies (Martínez-López and Zavala-Hidalgo, 2009; Muller-Karger et al., 2015). Overall strong positive Chl *a*-POC correlations (>0.6) were observed in Arabian Sea and in Regions A and D highlight phytoplankton biomass as a key carbon source, modulated by nutrient availability and hydrodynamic transport (Lee et al., 2020). However, terrigenous inputs and resuspended sediments complicate coastal POC-Chl *a* relationships (Holser et al., 2011). Moderate SST-POC linkages (>0.5) in Regions A and C emphasize temperature-dependent microbial respiration and particle degradation (Gardner et al., 2006), while POC showed a robust negative correlation with SST (-0.72, P<0.05) across the Arabian Sea. In previous findings, the light and nutrient availability also a key factor for phytoplankton growth (Krumhardt et al., 2017) and the role of wind-driven upwelling in regulating productivity (Krishna et al., 2023). However, MLD-POC coupling in Region C suggests wind-driven mixing regulates nutrient entertainment, being consistent with global models (Stramska, 2009).

The spatiotemporal variability across the Arabian Sea is closely linked to seasonal monsoonal circulations. The elevated SSS in the Arabian Sea, particularly due the pre-monsoon season, is largely driven by strong evaporative conditions and limited freshwater input. During the southwest monsoon season, the high-salinity surface waters are advected southeastward along the west coast of India, as described by Shenoi et al. (2005). Moreover, the Iranian water (Persian Gulf) regions serve as a major source of highly saline water masses that enter the Arabian Sea. The transport and dispersion of these saline intrusions are modulated by regional circulation, lateral mixing, and other processes, which collectively influence the spatial and temporal salinity structure of the Arabian Sea (Prasad et al., 2001; Swift and Bower, 2003). The Oman coast, influenced by strong monsoon-induced upwelling, facilitates vertical mixing and promotes high biological productivity (Chinta et al., 2024). The northern Arabian Sea benefit from rich in marine primary productivity due to freshwater inflow from Indus River and strong mixing from Balochistan coast (Kalhoro et al., 2025b). Shifts in the phytoplankton community composition, driven by physical and biogeochemical processes, further affect the Chl *a*-POC relationships (Vijayan et al., 2021). These data products provide valuable insights into the magnitude and trends of POC concentrations, offering a basis for understanding the oceanic biogeochemical cycles at both basin and global scale (Stramski et al., 2022). The observed decline in POC in the Arabian Sea parallels global reductions in primary productivity, driven by warming, stratification, and anthropogenic pressures. Coastal zones play a vital role in ocean productivity but are increasingly threatened by eutrophication and habitat loss. These findings underscore the importance of sustained monitoring to improve climate models and inform mitigation strategies in this sensitive region.

This study provides the values insights into the decadal trends of POC in the Arabian Sea and its key environmental drivers. However, several limitations must be considered. The BG algorithm, although effective for estimating surface POC, is inherently empirical and sensitive to regional bio-optical conditions. This sensitivity can introduce biases, particularly in complex regions with varying bio-optical properties. The use of decadal satellite data, while advantageous for analyzing large-scale trends, is limited by the algorithms sensitivity to changes in environmental factors, which can affect the accuracy of long-term assessments. Additionally, the lack of extensive high-resolution in-situ validation data further constrains the ability to assess the accuracy of satellite-derived POC estimates, especially in coastal regions where bio-optical properties can vary significantly. More in-situ data is needed to better validate satellite data to improve the reliability of POC estimates, particularly in dynamic coastal environments. To improve the robustness of these estimates, future research should focus on acquiring high-resolution in-situ observations for better validation the satellite data and refinement of the algorithm. Furthermore, the integration of coupled physical-biogeochemical models would be crucial for capturing the complex interactions between environmental variables and improving the mechanistic understanding of POC dynamics, particularly under dynamic conditions such as monsoonal winds and cyclonic events.

5 CONCLUSION

POC serves as critical component of marine biogeochemical cycles, reflecting primary productivity and carbon export dynamics essential for global carbon sequestration. This study elucidates the spatiotemporal variability of POC in the Arabian Sea using two decades (2001–2021) of satellite-derived and in-situ data from the PISCES biogeochemical model. Surface POC concentrations exhibited pronounced seasonality, peaking in winter due to convective mixing and during the southwest monsoon via wind-driven upwelling. Coastal zones consistently retained higher POC levels compared to offshore regions. This pattern reflects the influence of terrestrial inputs and nutrient-rich upwelling. Offshore regions showed reduced POC due to monsoon-related stratification. Vertical profiles revealed surface POC maxima (0–50 m; ≤50 mg/m^3), declining sharply below 100 m (≤21 mg/m^3), with a mid-depth resurgence (150–350 m; ≤25 mg/m^3) attributed to sinking organic aggregates from surface blooms. A strong positive Chl *a*-POC correlation (>0.6) affirmed that phytoplankton biomass is the primary driver of surface carbon variability, while weaker correlations with salinity, nutrients, and dissolved oxygen highlighted the secondary role of abiotic factors. Seasonal SST fluctuations (23–32 °C) and MLD variations further modulated vertical nutrient entrainment and carbon export efficiency. POC displayed moderate negative correlations with SSS, PAR, and WS while positively correlated with MLD in the Arabian Sea. The findings underscore the Arabian Sea sensitivity to monsoon dynamics and warming-induced stratification, which threaten to alter productivity and carbon sequestration capacity. Investigating regional-scale changes in POC and the impact of key oceanic drivers on its variability is crucial for understanding the broader biogeochemical implications for the Arabian Sea. Integration of satellite and vertical profile data enhances mechanistic understanding of marine carbon cycling, emphasizing the importance of sustained monitoring to predict ecosystem responses to climate and anthropogenic stressors in this biogeochemically pivotal region.

6 DATA AVAILABILITY STATEMENT

Monthly MODIS-Aqua POC and PAR spatial data, with 4-km resolution was obtained from NASA OceanColor Web platform L3 (https://oceancolor.gsfc.nasa.gov/l3/order/), and monthly spatial distribution and vertical profile data for POC, Chl *a*, SST, SSS, pH, NO_3, PO_4, O_2, Si were derived from Copernicus Marine and Environment Monitoring Service (CMEMS) (https://data.marine.copernicus.eu/products).

7 ACKNOWLEDGMENT

We thank the data supports from National Marine Scientific Data Center (Dalian), the National Science & Technology Infrastructure of China (http://odc.dlou.edu.cn/), Liaoning Marine Scientific Data Center, and the Dalian Marine Scientific Data Center for providing valuable data and information. We also thank the reviewers for carefully reviewing the manuscript and providing valuable comments to help improve this paper.

References

Bhattathiri P M A, Pant A, Sawant S S et al. 1996. Phytoplankton production and chlorophyll distribution in the eastarn and central Arabian Sea in 1994-1995. *Current Science*, **71**(11): 857-862.

Böhm E, Morrison J M, Manghnani V et al. 1999. The Ras Al Hadd Jet: remotely sensed and acoustic Doppler current profiler observations in 1994-1995. *Deep Sea Research Part II*: *Topical Studies in Oceanography*, **46**(8-9): 1531-1549, https://doi.org/10.1016/S0967-0645(99)00034-X.

Chinta V, Kalhoro M A, Liang Z L et al. 2024. Decadal climate variability of chlorophyll-*a* in response to different oceanic factors in the Western Indian Ocean: the Sea of Oman. *Climate Dynamics*, **62**(9): 8675-8690, https://doi.org/10.1007/s00382-024-07354-4.

Chinta V, Kalhoro M A, Tahir M et al. 2025. Impact of tropical cyclone Tej on oceanic environment in the Arabian Peninsula. *Frontiers in Marine Science*, **12**, https://doi.org/10.3389/fmars.2025.1575203.

Chiswell S M, Sutton P J H. 2020. Relationships between long-term ocean warming, marine heat waves and primary production in the New Zealand region. *New Zealand Journal of Marine and Freshwater Research*, **54**(4): 614-635, https://doi.org/10.1080/00288330.2020.1713181.

Dobashi R, Ueno H, Matsudera N et al. 2022. Impact of mesoscale eddies on particulate organic carbon flux in the western subarctic north Pacific. *Journal of Oceanography*, **78**(1): 1-14, https://doi.org/10.1007/s10872-021-00620-7.

Ducklow H W, Steinberg D K, Buesseler K O. 2001. Upper Ocean carbon export and the biological pump. *Oceanography*, **14**(4): 50-58, https://doi.org/10.5670/oceanog.2001.06.

Evers-King H, Martinez-Vicente V, Brewin R J W et al. 2017. Validation and intercomparison of ocean color algorithms for estimating particulate organic carbon in the oceans. *Frontiers in Marine Science*, **4**: 251, https://doi.org/10.3389/fmars.2017.00251.

Fan H, Wang X J, Zhang H B et al. 2018. Spatial and temporal variations of particulate organic carbon in the Yellow-Bohai Sea over 2002 2016. *Scientific Reports*, **8**(1): 7971, https://doi.org/10.1038/s41598-018-26373-w.

Fernandes L, Bhosle N B, Matondkar S G P et al. 2009. Seasonal and spatial distribution of particulate organic matter in the Bay of Bengal. *Journal of Marine Systems*, **77**(1-2): 137-147, https://doi.org/10.1016/J.JMARSYS.2008.12.002.

Fingas M. 2019. Remote sensing for marine management. *In*: Sheppard C ed. World Seas: An Environmental Evaluation. Volume III: Ecological Issues and Environmental Impacts. 2nd edn. Elsevier, Amsterdam. p.103-119, https://doi.org/10.1016/b978-0-12-805052-1.00005-x.

Fox-Kemper B, Hewitt H T, Xiao C D et al. 2021. Ocean, Cryosphere and Sea Level Change, in: Climate Change 2021: The Physical Science Basis, Contribution of Working Group I to the Sixth Assessment Report of the Intergovernmental Panel on Climate Change. *In*: Masson-Delmotte V, Zhai P, Pirani A et al. Cambridge University Press, Cambridge, UK and New York, NY, USA, p.1211-1362, https://doi.org/10.1017/9781009157896.011, 2021.

Gardner W D, Mishonov A V, Richardson M J. 2006. Global POC concentrations from in-situ and satellite data. *Deep Sea Research Part II*: *Topical Studies in Oceanography*, **53**(5-7): 718-740, https://doi.org/10.1016/j.dsr2.2006.01.029.

Giraud X, Le Quéré C, da Cunha L C. 2008. Importance of coastal nutrient supply for global ocean biogeochemistry. *Global Biogeochemical Cycles*, **22**(2): GB2025, https://doi.org/10.1029/2006GB002717.

Gomes H R, Goes J I, Saino T. 2000. Influence of physical processes and freshwater discharge on the seasonality of phytoplankton regime in the Bay of Bengal. *Continental Shelf Research*, **20**(3): 313-330, https://doi.org/10.1016/S0278-4343(99)00072-2.

Gopalakrishna V V, Murty V S N, Sengupta D et al. 2002. Upper ocean stratification and circulation in the northern Bay of Bengal during southwest monsoon of 1991. *Continental Shelf Research*, **22**(5): 791-802, https://doi.org/10.1016/S0278-4343(01)00084-X.

Holser R R, Goni M A, Hales B. 2011. Design and application of a semi-automated filtration system to study the distribution of particulate organic carbon in the water column of a coastal upwelling system. *Marine Chemistry*, **123**(1-4): 67-77, https://doi.org/10.1016/j.marchem.2010.10.001.

Honjo S, Eglinton T I, Taylor C D et al. 2014. Understanding the role of the biological pump in the global carbon cycle: an imperative for ocean science. *Oceanography*, **27**(3): 10-16, https://doi.org/10.2307/24862184.

Jahnke R A. 1996. The global ocean flux of particulate organic carbon: areal distribution and magnitude. *Global Biogeochemical Cycles*, **10**(1): 71-88, https://doi.org/10.1029/95GB03525.

Johns W E, Yao F, Olson D B et al. 2003. Observations of seasonal exchange through the Straits of Hormuz and the inferred heat and freshwater budgets of the Persian Gulf. *Journal of Geophysical Research*: *Oceans*, **108**(C12): 3391, https://doi.org/10.1029/2003JC001881.

Kalhoro M A, Chinta V, de Mutsert K et al. 2024. Impact of tropical cyclone Biparjoy on oceanic parameters in the Arabian Sea. *Marine Pollution Bulletin*, **208**: 117046, https://doi.org/10.1016/j.marpolbul.2024.117046.

Kalhoro M A, Chinta V, Tahir M et al. 2025a. Assessing chlorophyll-*a* variability and its relationship with decadal climate patterns in the Arabian Sea. *Journal of Marine Science and Engineering*, **13**(6): 1170, https://doi.org/10.3390/jmse13061170.

Kalhoro M A, Ye H J, Liu C L et al. 2025b. Impact of sea surface temperature fronts on the spatial distribution of jellyfish in the northern Arabian Sea. *Estuarine*, *Coastal and Shelf Science*, **312**: 109033, https://doi.org/10.1016/j.ecss.2024.109033.

Kandasamy P, Sarangi R K, Ayyappan S et al. 2019. Influence of sea surface temperature and chlorophyll-*a* on the distribution of particulate organic carbon in the southwest Bay of Bengal. *Journal of Geomatics*, **13**(2): 291-303.

Karp-Boss L, Wheeler P A, Hales B et al. 2004. Distributions and variability of particulate organic matter in a coastal upwelling system. *Journal of Geophysical Research*: *Oceans*, **109**(C9): C09010, https://doi.org/10.1029/2003JC002184.

Khan M, Liu Y K. 2019. Geodynamic evolution of the offshore Indus Basin Pakistan: the western Indian plate passive continental margin. *Geophysical Journal International*, **217**(2): 1366-1386, https://doi.org/10.1093/gji/ggz091.

Krishna L, Bharti R, Mahanta C. 2023. Significance of biological forcing on the spatio-temporal variability of carbon dioxide fluxes over the Northern Indian Ocean. *In*: Proceedings of EGU General Assembly 2023. EGU, Vienna, https://doi.org/10.5194/egusphere-egu23-15166.

Krumhardt K M, Lovenduski N S, Long M C et al. 2017. Avoidable impacts of ocean warming on marine primary production: insights from the CESM ensembles. *Global Biogeochemical Cycles*, **31**(1): 114-133, https://doi.org/10.1002/2016GB005528.

Le C F, Lehrter J C, Hu C M et al. 2017. Satellite observation of particulate organic carbon dynamics on the Louisiana continental shelf. *Journal of Geophysical Research*: *Oceans*, **122**(1): 555-569, https://doi.org/10.1002/2016JC012275.

Lee C M, Jones B H, Brink K H et al. 2000. The upper-ocean response to monsoonal forcing in the Arabian Sea: seasonal and spatial variability. *Deep Sea Research Part II*: *Topical Studies in Oceanography*, **47**(7-8): 1177-1226, https://doi.org/10.1016/S0967-0645(99)00141-1.

Lee D, Son S H, Joo H T et al. 2020. Estimation of the particulate organic carbon to chlorophyll-*a* ratio using MODIS-Aqua in the East/Japan sea, South Korea. *Remote Sensing*, **12**(5): 840, https://doi.org/10.3390/rs12050840.

Liu C L, Ma N N, Sun M et al. 2025. Impact of climate change on frequency and community structure of red tide events in the northern South China Sea. *Climate Dynamics*, **63**(1): 51, https://doi.org/10.1007/s00382-024-07552-0.

Liu D, Bai Y, He X Q et al. 2019. Satellite estimation of particulate organic carbon flux from Changjiang River to the estuary. *Remote Sensing of Environment*, **223**: 307-319, https://doi.org/10.1016/j.rse.2019.01.025.

Loisel H, Nicolas J M, Deschamps P Y et al. 2002. Seasonal and inter-annual variability of particulate organic matter in the global ocean. *Geophysical Research Letters*, **29**(24): 49-1-49-4, https://doi.org/10.1029/2002GL015948.

Mahar G A, Ahmed R, Iqbal M J et al. 2019. Tsunami threat versus development activities along the coast of Pakistan: a geographic assessment. *Global NEXT Journal*, **21**(3): 347-354, https://doi.org/10.30955/gnj.002878.

Mahar G A. 2010. Geomorphic Degradation of Indus Delta and its Demographic Impact. University of Karachi, Karachi.

Martínez-López B, Zavala-Hidalgo J. 2009. Seasonal and interannual variability of cross-shelf transports of chlorophyll in the Gulf of Mexico. *Journal of Marine Systems*, **77**(1-2): 1-20, https://doi.org/10.1016/j.jmarsys.2008.10.002.

Muller-Karger F E, Smith J P, Werner S et al. 2015. Natural variability of surface oceanographic conditions in the offshore Gulf of Mexico. *Progress in Oceanography*, **134**: 54-76, https://doi.org/10.1016/j.pocean.2014.12.007.

O'Reilly J E, Werdell P J. 2019. Chlorophyll algorithms for ocean color sensors—OC4, OC5 & OC6. *Remote Sensing of Environment*, **229**: 32-47, https://doi.org/10.1016/j.rse.2019.04.021.

Parvaresh A, Hassanzadeh S, Bordbar M H. 2005. Statistical analysis of wave parameters in the north coast of the Persian Gulf. *Annales Geophysicae*, **23**(6): 2031-2038, https://doi.org/10.5194/angeo-23-2031-2005.

Patra P K, Kumar M D, Mahowald N et al. 2007. Atmospheric deposition and surface stratification as controls of contrasting chlorophyll abundance in the North Indian. *Journal of Geophysical Research*: *Oceans*, **112**(C5): C05029, https://doi.org/10.1029/2006JC003885.

Prakash P, Prakash S, Rahaman H et al. 2012. Is the trend in chlorophyll-*a* in the Arabian Sea decreasing? *Geophysical Research Letters*, **39**(23): L23605, https://doi.org/10.1029/2012GL054187.

Prasad T G, Ikeda M, Kumar S P. 2001. Seasonal spreading of the Persian Gulf water mass in the Arabian Sea. *Journal of Geophysical Research*: *Oceans*, **106**(C8): 17059-17071, https://doi.org/10.1029/2000JC000480.

Ramaiah N, Raghukumar S, Gauns M. 1996. Bacterial abundance and production in the central and eastern Arabian Sea. *Current Science*, **71**(11): 878-882.

Roman M, Smith S, Wishner K et al. 2000. Mesozooplankton production and grazing in the Arabian Sea. *Deep Sea Research Part II*: *Topical Studies in Oceanography*, **47**(7-8): 1423-1450, https://doi.org/10.1016/S0967-0645(99)00149-6.

Rouf M A, Golder M R, Sumana Z A. 2021. Satellite-based observation of particulate organic carbon in the northern Bay of Bengal. *Environmental Advances*, **6**: 100124, https://doi.org/10.1016/j.envadv.2021.100124.

Roxy M K, Modi A, Murtugudde R et al. 2016. A reduction in marine primary productivity driven by rapid warming over the tropical Indian Ocean. *Geophysical Research Letters*, **43**(2): 826-833, https://doi.org/10.1002/2015GL066979.

Sarin M M, Rengarajan R, Ramaswamy V. 1996. ^{234}Th scavenging and particle export fluxes from the upper 100 m of the Arabian Sea. *Current Science*, **71**(11): 888-893.

Shaju S S, Sunny G M, Sherin C K et al. 2022. Variability of particulate organic carbon and assessment of satellite retrieval algorithms over the eastern Arabian Sea. *Environmental Monitoring and Assessment*, **194**(9): 656, https://doi.org/10.1007/s10661-022-10264-9.

Shen Z L, Yang H M, Liu Q. 2020. Particulate organic carbon and its composition in Jiaozhou Bay. *In*: Shen Z L ed. Studies of the Biogeochemistry of Typical Estuaries and Bays in China. Springer, Berlin, Heidelberg. p.227-235, https://doi.org/10.1007/978-3-662-58169-8_14.

Shenoi S, Shankar D, Gopalakrishna V et al. 2005. Role of ocean in the genesis and annihilation of the core of the warm pool in the southeastern Arabian Sea. *Mausam*, **56**(1): 147-160.

Shetye S R, Gouveia A D, Shenoi S S C. 1994. Circulation and water masses of the Arabian Sea. *Proceedings of the Indian Academy of Sciences-Earth and Planetary Sciences*, **103**(2): 107-123, https://doi.org/10.1007/BF02839532.

Son Y B, Gardner W D, Mishonov A V et al. 2009. Multispectral remote-sensing algorithms for particulate organic carbon (POC): the Gulf of Mexico. *Remote Sensing of Environment*, **113**(1): 50-61, https://doi.org/10.1016/j.rse.2008.08.011.

Stramska M, Cieszyńska A. 2015. Ocean colour estimates of particulate organic carbon reservoirs in the global ocean-revisited. *International Journal of Remote Sensing*, **36**(14): 3675-3700, https://doi.org/10.1080/01431161.2015.1049380.

Stramska M, Stramski D. 2005. Variability of particulate organic carbon concentration in the north polar Atlantic based on ocean color observations with Sea-viewing Wide Field-of-view Sensor (SeaWiFS). *Journal of Geophysical Research*: *Oceans*, **110**(C10): C10018, https://doi.org/10.1029/2004JC002762.

Stramska M. 2009. Particulate organic carbon in the global ocean derived from SeaWiFS ocean color. *Deep Sea Research Part I*: *Oceanographic Research Papers*, **56**(9): 1459-1470, https://doi.org/10.1016/J.DSR.2009.04.009.

Stramska M. 2014. Particulate organic carbon in the surface waters of the North Atlantic: spatial and temporal variability based on satellite ocean colour. *International Journal of Remote Sensing*, **35**(13): 4717-4738, https://doi.org/10.1080/01431161.2014.919686.

Stramski D, Joshi I, Reynolds R A. 2022. Ocean color algorithms to estimate the concentration of particulate organic carbon in surface waters of the global ocean in support of a long-term data record from multiple satellite missions. *Remote Sensing of Environment*, **269**: 112776, https://doi.org/10.1016/j.rse.2021.112776.

Stramski D, Reynolds R A, Babin M et al. 2008. Relationships between the surface concentration of particulate organic carbon and optical properties in the eastern South Pacific and eastern Atlantic Oceans. *Biogeosciences*, **5**(1): 171-201, https://doi.org/10.5194/bg-5-171-2008.

Swift S A, Bower A S. 2003. Formation and circulation of dense water in the Persian/Arabian Gulf. *Journal of Geophysical Research*: *Oceans*, **108**(C1): 3004, https://doi.org/10.1029/2002JC001360.

Świrgoń M, Stramska M. 2015. Comparison of in situ and satellite ocean color determinations of particulate organic carbon concentration in the global ocean. *Oceanologia*, **57**(1): 25-31, https://doi.org/10.1016/j.oceano.2014.09.002.

Thomsen L, Aguzzi J, Costa C et al. 2017. The oceanic biological pump: rapid carbon transfer to depth at continental margins during winter. *Scientific Reports*, **7**(1): 10763, https://doi.org/10.1038/s41598-017-11075-6.

Valsala V, Murtugudde R. 2015. Mesoscale and intraseasonal air-sea CO_2 exchanges in the western Arabian Sea during boreal summer. *Deep Sea Research Part I*: *Oceanographic Research Papers*, **103**: 101-113, https://doi.org/10.1016/j.dsr.2015.06.001.

Vijayan A K, Reddy B B, Sudheesh V et al. 2021. Phytoplankton community structure in a contrasting physico-chemical regime along the eastern Arabian Sea during the winter monsoon. *Journal of Marine Systems*, **215**: 103501, https://doi.org/10.1016/j.jmarsys.2020.103501.

Wang C L, Hao Z, Gao J H et al. 2020. Reservoir construction has reduced organic carbon deposition in the East China Sea by half since 2006. *Geophysical Research Letters*, **47**(17): e2020GL087357, https://doi.org/10.1029/2020GL087357.

Wang X C, Ma H Q, Li R H et al. 2012. Seasonal fluxes and source variation of organic carbon transported by two major Chinese Rivers: the Yellow River and Changjiang (Yangtze) River. *Global Biogeochemical Cycles*, **26**(2): GB2025, https://doi.org/10.1029/2011gb004130.

Wei X D, Shen F, Pan Y Q et al. 2019. Satellite observations of the diurnal dynamics of particulate organic carbon in optically complex coastal oceans: the continental shelf seas of China. *Journal of Geophysical Research*: *Oceans*, **124**(7): 4710-4726, https://doi.org/10.1029/2018JC014715.

Xu K H, Milliman J D. 2009. Seasonal variations of sediment discharge from the Yangtze River before and after impoundment of the Three Gorges Dam. *Geomorphology*, **104**(3-4): 276-283, https://doi.org/10.1016/j.geomorph.2008.09.004.

Yu J, Wang X J, Fan H et al. 2019. Impacts of physical and biological processes on spatial and temporal variability of particulate organic carbon in the North Pacific Ocean during 2003-2017. *Scientific Reports*, **9**(1): 16493, https://doi.org/10.1038/s41598-019-53025-4.

Zhu G H, Liu Y L, Chen L H et al. 2011. Studies on phytoplankton and particulate organic carbon in the southern Ocean. *Applied Mechanics and Materials*, **137**: 344-352, https://doi.org/10.4028/www.scientific.net/amm.137.344.

Electronic supplementary material

Supplementary material (Supplementary Figs.S1–S4) is available in the online version of this article at https://doi.org/10.1007/s00343-025-5092-2.